PROCEEDINGS OF SPIE

SPIEDigitalLibrary.org/conference-proceedings-of-spie

Calculation of signals for oceanographic lidar

Kunal Mitra
James H. Churnside

SPIE.

Calculation of signals for oceanographic lidar

Kunal Mitra[a] and James H. Churnside[b]

[a] Florida Institute of Technology, Melbourne, FL 32901
[b] National Oceanic and Atmospheric Administration, ETL, Boulder, CO 80303

ABSTRACT

This paper calculates signal levels that would be obtained from oceanographic lidar by solving the one-dimensional transient radiative transfer equation for remote sensing. As an example, detection of fish schools is considered. In this technique a pulsed laser is directed into the ocean, and the time-dependent back-scattered flux is measured at different locations. A large number of parameters such as the spatial and temporal variability of optical properties within the ocean, ocean depth, type of ocean water, and presence of biological matters can significantly affect the radiative transport through oceans. But since the emphasis of the work is on the scattering phenomenon, important parameters associated with it, namely the scattering albedo and scattering phase function distribution, are considered in detail.

Keywords: Ocean optics, transient radiative transfer, lidar, fisheries

1. INTRODUCTION

Most of the work in radiative transfer in the ocean has been directed toward understanding the propagation of sunlight.[1] For these applications, the transient term in the radiative transfer equation can be neglected. The justification for this assumption is that changes in the incident illumination are much slower than the changes imposed by the propagation of the light field through the medium. The assumption is clearly satisfied for solar illumination. However, lidar systems may use pulses that are shorter than the attenuation distance of sea water divided by the speed of light in water. Because of multiple scattering, light will be present at any given depth after the unscattered pulse has gone past. Understanding the lidar signal, therefore, requires solution of the time-dependent radiative transfer equation.

The Monte Carlo method is the most common technique used for both steady state and transient radiative transfer in the ocean.[1,2] This has proven to be an extremely powerful technique. It is well-suited to the use of empirical values for the properties of the medium. The errors in the results are unbiased and well-understood. Implementation of this technique is relatively straight-forward. However, it also has a couple of shortcomings. It tends to be computationally intensive, especially for lidar applications, where few of the initial photons contribute to the signal. In some cases, the relative importance of various processes is difficult to infer from a Monte Carlo calculation. The discrete ordinate method has also been used to analyze the steady state problem in sea water.[1,3]

Different techniques to solve the transient radiative transfer equation have been developed. These include spherical harmonics expansion, discrete ordinates, and direct numerical integration. Some of this development has been stimulated by the progress in time-resolved optical tomography[4,5] of living tissues and organs using short light pulses. This technology has the potential to provide physiological and morphological information to medical practitioners without some of the problems associated with harmful radiation, in the case of x-rays, or with harmful chemicals, in the case of positron tomography and single-photon-emission tomography.

Like sea water, biological tissue is a propagation medium that both scatters and absorbs visible light. For the case of a short pulse laser, the radiation signal of interest is the scattered intensity that persists for long periods due to multiple scattering after the initial pulse has been shut off. The advantage of performing transient analysis is the additional information about medium properties that is obtained from the measured signal.[6]

Part of the SPIE Conference on Advances in Laser Remote Sensing for Terrestrial and Hydrographic Applications
Orlando, Florida • April 1998 SPIE Vol. 3382 • 0277-786X/98/$10.00

This paper considers discrete ordinate solutions to the transient radiative transfer equation in one dimension. A pulse shape typical of a Q-switched laser is used. Two general problems are treated. The first case corresponds to a uniform ocean with various scattering parameters. The Henyey-Greenstein distribution is used to approximate the scattering phase function[7] and the effects of different albedo and asymmetry are investigated. This investigation demonstrates that the attenuation of a lidar signal can be less than the diffuse attenuation coefficient for the one-dimensional geometry.

The second problem is one where in the ocean a discrete layer having different optical properties is present. As an example, properties representative of a school of small fish are considered. Aerial lidar is being considered for fish detection and for biomass surveys due to the difficulties and expenses encountered with more traditional surveying such as ichthyoplankton sampling, trawling, and acoustic surveying.[8,9] In the tuna industry, improved techniques for locating schools that are not associated with dolphins can reduce dolphin mortality during fishing operations. In epipelagic fisheries, such as those for anchovies, sardines, menhaden, and herring, the increasing costs of traditional ship-based survey techniques and the increasing requirements for accurate stock measurements are generating interest in lidar as a fisheries management tool.

Aerial detection of fish has been demonstrated and single-scattering and Monte Carlo models have been applied to analyze lidar performance.[2,10,11] Here the results of the discrete ordinate solution are presented. The scattering properties of fish are assumed to be the same as diffuse spheres of equivalent cross-sectional area. We find that the detection of fish in water depends on the scattering phase function distribution and the optical properties of the water.

2. THEORETICAL DEVELOPMENT

The physical case under consideration is a one-dimensional scattering and absorbing layered ocean medium with depth L, infinite horizontal extent, and azimuthal symmetry. As an example, fish layers having different properties from those of small particles (including mineral sediments, phytoplankton, and zooplankton) are present in the ocean between a depth of L_1 and $L_1 + L_2$ from the ocean surface (see Fig. 1). For simplicity, the boundaries of the medium are considered to be non-reflecting and non-refracting. This geometry is the simplest possible and therefore is chosen in order to examine the effects of various approximations with the least additional mathematical complexity. The radiative transfer equation in this geometry, assuming azimuthal symmetry and constant properties, is written as[12]

$$\frac{1}{c}\frac{\partial L(z,\mu,t)}{\partial t} + \mu\frac{\partial L(z,\mu,t)}{\partial z} = -k_e L(z,\mu,t) + \frac{k_s}{2}\int_{-1}^{1} L(z,\mu',t)\, p(\mu' \to \mu)\, d\mu' + S(z,\mu,t) \quad , \tag{1}$$

where L is the intensity ($\mathrm{Wm^{-2}sr^{-1}}$), c the speed of light in the medium, z the Cartesian distance, t the time, k the radiative attenuation coefficient, μ the cosine of θ where θ is the polar angle measured from the positive z-axis, and p the scattering phase function. The above is an integro-differential equation where the partial differentials represent a hyperbolic form of equation. The scattering phase function similar to that given in the literature[1] satisfies the normalization

$$\frac{1}{2}\int_0^{\pi} p(\theta)\sin\theta\, d\theta = 1 \quad . \tag{2}$$

The phase function in general can be represented in terms of a series of Legendre Polynomials P_m as[13]

$$p(\Theta) = \sum_{m=0}^{M} a_m P_m(\cos\Theta) \quad , \tag{3a}$$

where Θ is the scattering angle, M the order of anisotropy, and a_m are the coefficients in the expansion. The advantage of this formulation is that, for the one-dimensional plane-parallel geometry and azimuthal symmetry, the phase function depends only on the initial and final values of the polar angle, as[14]

$$\frac{1}{2\pi}\int_0^{2\pi} P_m(\cos\Theta)\, d\varphi = P_m(\mu')\, P_m(\mu) \quad , \quad \cos\Theta = \mu\mu' + \sqrt{1-\mu^2}\,\sqrt{1-\mu'^2}\cos(\varphi - \varphi') \quad , \tag{3b}$$

where φ is the azimuthal angle.

The phase function for particulates present in the ocean has been approximated by the Henyey-Greenstein expansion as[14]

$$p_p(\Theta) = \sum_{m=0}^{M} (2m+1)\, g^m\, P_m(\cos\Theta) \quad , \tag{4a}$$

where g is the asymmetry factor. Sometimes for a simpler analysis the directional scattering behavior is described by the asymmetric factor, which is the average cosine of the scattering angle. The asymmetry factor is related to the phase function by[14]

$$g = \frac{1}{2} \int_0^{\pi} p(\theta) \cos\theta \, d(\cos\theta) \quad . \tag{4b}$$

Petzold measured the phase function of a typical ocean water.[7] Unfortunately, there is no value of g that represents Petzold's phase function accurately both in the forward and backward directions. Also, the phase function measured by Petzold is highly forward-scattered and a large number of coefficients have to be retained in the expansion, as given by Eq. (3a) for accurate modeling of the phase function. A plot showing the Petzold measured phase function distribution and that for values of asymmetry factor equal to 0.25, 0.5, 0.75, and 0.87 for Henyey-Greenstein phase function distribution is shown in Fig. 2. Higher values of g correspond to more forward-peaked phase function distributions, so the magnitude of these Henyey-Greenstein phase functions match the Petzold function better near μ = 1. But the Henyey-Greenstein function overestimates the phase function distribution in the backward directions.

For the case of fish, the phase function can be adequately represented by Eq. (3a). The coefficients a_m are calculated as given by[15] using the phase function distribution for large diffusing spheres derived from geometric optics theory[14]

$$p_f(\theta) = \frac{8}{3\pi} (\sin\Theta - \Theta\cos\Theta) \quad . \tag{5}$$

This phase function for fish is an approximate one but it is chosen since the expression is free of any parameters that depend on fish properties and it is reasonable to approximate the fish as large diffusing spheres for analysis purpose.

In the traditional transient radiative transport equation, the first term on the left in Eq. (1) is neglected because of the large value of c. The intensity I remains time-dependent, but the time variation in traditional model is introduced only through the time-dependent boundary conditions or the time-dependent source.

The equation of transfer is complicated because of the integral on the right side corresponding to the in-scattering gain term. In order to reduce the integral to a simpler form, different approximations such as spherical harmonics expansion, discrete ordinate method, and direct numerical integration technique were used. But it was found during computation that the spherical harmonics method yielded unrealistic results for the individual components of the intensity in any particular direction (for example, the direct back-scatter component for the lidar), although it was quite accurate for prediction of the integrated values of the intensity over all back-scattered directions. Since in a lidar one is interested in the back-scatter component $\theta = \pi$, the spherical harmonics method is not used for analysis of this problem. Direct numerical integration was found to be very expensive from computational point of view compared to the discrete ordinate method because of the higher number of angular directional nodes required to obtain the correct solution. The discrete ordinate method is based on a weighted, non-uniform discrete representation of the directional variation of the radiation intensity; therefore accurate solutions are obtained using fewer angular directional nodes. Therefore, the focus in this paper is on the discrete ordinate method of solving the transient radiative transfer equation.

The method of discrete ordinates replaces the integral on the right hand side of Eq. (1) by a quadrature, such as Gaussian, Lobatto, or Chebyshev.[16,17] If μ_i's are the quadrature points between the limits of integration, -1 to 1, corresponding to a $2K$ -order quadrature, and w_i's are the corresponding weights, the equation is reduced to the following system of coupled hyperbolic partial differential equations

$$\frac{1}{c}\frac{\partial L_i(z,t)}{\partial t}+\mu_i\frac{\partial L_i(z,t)}{\partial z}=-k_e L_i(z,t)+\frac{k_s}{2}\sum_{j=-K}^{K} w_j L_j(z,t)\,p(\mu_j\rightarrow\mu_i)+S(z,\mu_i,t)\quad,\quad i,j\neq 0\quad, \tag{6}$$

where $L_i(z,t) = L(z, \mu_i, t)$. The Gaussian quadrature of even order was used to avoid the value $\mu = 0$.

3. SOURCE PULSE AND BOUNDARY CONDITIONS

The propagating pulsed source considered in this study is a pulsed laser with a fast rise and an exponentially decaying tail, which is typical of a Q-switched laser. The intensity in the medium can be separated into a collimated component, corresponding to the incident source, and a scattered intensity. If the collimated intensity is L_c then L is the remaining part which can be described by Eq. (1). The collimated component of the intensity, L_c, is represented by

$$L_c(z,\mu,t)=L_{incident}\exp(-k_e z)\,(t-z/c)\exp[-(t-z/c)/\tau]\,H(t-z/c)\,\delta(\mu-1)\quad, \tag{7a}$$

where $L_{incident}$ is the peak power at the surface, $H(t)$ the Heavyside step function and $\delta(t)$ the Dirac delta function.

The source function S for the scattered intensity field is then given by

$$S(z,\mu,t)=\frac{k_s}{2}\int_{-1}^{1} L_c(z,\mu',t)\,p(\mu'\rightarrow\mu)\,d\mu'\quad, \tag{7b}$$

where τ is 0.408 times the pulse width at half maximum, which equals 10 *ns* in this paper.

The boundary conditions are such that the intensities pointing inward at $z = 0$ and $z = L$ are zero, yielding

$$I(z=0,\mu>0,t)=I(z=L,\mu<0,t)=0\quad. \tag{8}$$

The intensities at the interfaces $z = L_1$ and $z = L_2$ are assumed to be continuous.

4. OPTICAL PROPERTIES USED

The scattering and absorbing properties of fish are calculated using the following relations:

$$k_s=2RAl^2N\quad, \tag{9a}$$

$$k_a=2(1-R)Al^2N\quad, \tag{9b}$$

where A is the aspect ratio, N the school density, l the fish length, and R the reflectivity. In this analysis, values of A, R, and l used are 0.1, 19.5 %, and 15 *cm*, which are typical of sardines.[9,18] The range of number density of sardines N is varied from 4 to 400 m^{-3}. The aspect A is calculated by dividing the cross-sectional area of the fish by the square of the fish length. The reflectivity of the unpolarized light R is calculated from the measurements of co-polarized and cross-polarized values.[9]

The optical properties of the water depend upon the type of ocean water used. For this analysis, various types of ocean water ranging from clear water (lower albedo) to turbid water (high albedo) are considered.[7]

5. RESULTS AND DISCUSSIONS

The numerical solutions for discrete ordinates method are obtained using the subroutine PDECOL.[18] For all simulations, the grid sizes for both time and space variables are varied by one order in either direction from the used values, and the results are found to be stable and converging.

The results and discussions are broadly divided into two sub-sections. In section 5.1 the effects of the various types of ocean water on the measured back-scattered signal are analyzed. Section 5.2 deals with the effects on the back-scattered signals due to the presence of schools of fish having different number density, location, and width. In order to measure the direct back-scatter component the measurements have to be performed at $\mu = -1$.

5.1. Effect of Various Types of Ocean Water on the Measured Signal

The results of the back-scattered flux for the case of ocean water having $g = 0.5$ and containing no fish is considered as the base curve. Though a higher value of g, such as 0.75 or 0.87, is a better representation of the water particles as discussed in the previous section, a value of $g = 0.5$ is used as a base case for convenience from a computational point of view. Since a higher value of asymmetric factor implies a more forward-scattered phase function distribution, more discrete ordinates will be required for accurate prediction of back-scattered flux. For twelve discrete ordinates, the most backward and forward directions are equal to -0.985 and 0.985. As the number of discrete ordinates is increased, the most forward and backward directional nodes approach unity.

Figure 3 represents the comparison of the back-scattered flux at $\mu = -0.985$ for various types of ocean water, ranging from lower to higher optical albedo (ω), using the twelve discrete ordinates and $g = 0.5$. The four different types of ocean water considered have the following optical properties: (i) $k_s = 0.037\ m^{-1}$, $k_a = 0.114\ m^{-1}$ ($\omega = 0.245$); (ii) $k_s = 0.1\ m^{-1}$, $k_a = 0.12\ m^{-1}$ ($\omega = 0.454$); (iii) $k_s = 0.219\ m^{-1}$, $k_a = 0.179\ m^{-1}$ ($\omega = 0.551$); (iv) $k_s = 1.824\ m^{-1}$, $k_a = 0.366\ m^{-1}$ ($\omega = 0.833$). The varieties of water mentioned above represent a wide spectrum ranging from clear ocean to turbid harbor, as given in the literature.[7] The magnitude of the back-scattered flux for higher albedo is higher than that of the lower albedo near the surface, but it drops more sharply with depth because the source pulse decays correspondingly faster for higher albedo. The slopes of the lines plotted in Fig. 3 yield the lidar attenuation coefficients (α) for the different types of ocean water and are given in Table 1.

In fact, the lidar attenuation coefficient obtained for $g = 0.75$ and 0.87 is less than the absorption coefficient for lower albedo, as can be seen in Table 1. This is due to the fact that for higher values of g the phase function distribution in the backward direction ($\mu = -1$) decreases, as can be seen in Fig. 2, and lower albedo implies fewer scattering events. Therefore the effective scattering coefficient attains a negative value which tends to lower the magnitude of the lidar attenuation coefficient even lower than the absorption coefficient in the case of water with lower albedo and high value of asymmetric factor. This has been thoroughly tested but, for purpose of brevity, the results are not presented here.

The diffuse attenuation coefficient k_d is defined as the rate of change of downwelling intensity with depth.[19] For this calculation, the time-averaged forward-directed intensities are calculated at different depths for different types of water. The results of the diffuse attenuation coefficient obtained by time-averaging of the transient model match the results obtained by the steady-state calculations. The diffuse attenuation coefficient varies with depth. The value of k_d presented in Table 1 is calculated between a depth of 25 to 30 m. The diffuse attenuation coefficient $\hat{k}_d$ is also calculated on the basis of the quasi-single-scattering approximation.[20] This is represented as the sum of the absorption coefficient (k_a) and the back-scatter coefficient (b_b) obtained by integrating the volume scattering phase function from $\mu = -1$ to 0. Table 1 shows the values of the k_d and $\hat{k}_d$ for the various types of ocean water. It can be seen that broader phase function distributions (i.e. lower values of g) produce higher values of k_d and $\hat{k}_d$ for all types of water. The value of k_d is also greater than $\hat{k}_d$ except for the low albedo case. The diffuse attenuation coefficient is also greater than the lidar attenuation coefficient, contrary to the steady state case, except for lower albedo water. For transient analysis due to multiple scattering effects, more signal reaches back to the detector, thereby increasing the back-scattered signal and lowering the lidar attenuation coefficient.

Figure 4 shows the comparison of the back-scattered signal as a function of depth for values of g equal to 0.25, 0.5, 0.75, and 0.87. The different parameters used are $k_s = 0.1\ m^{-1}$, $k_a = 0.12\ m^{-1}$, and $L = 50\ m$. This is done to examine the effect of phase function on the back-scattered flux. The magnitude of the back-scattered flux increases with the decrease of g. This is because the lower value of asymmetric factor g implies a broader phase function distribution and is less forward-peaked in nature. The ratios of the peak magnitudes for different values of g are similar to those of the phase function distribution near $\mu = -1$ obtained from Fig. 2.

5.2. Effects of Presence of Fish in Ocean Water

The effects of number density, thickness of schools of fish, and distance of schools of fish from the ocean surface on the back-scattered flux are analyzed in this section. A value of $g = 0.87$ is used in this section (except in Fig. 5a) in order to show the pronounced effect of the presence of fish in the water. The optical properties of the ocean water used are $k_s = 0.1$ m^{-1} , $k_a = 0.12$ m^{-1}; the school density of fish (N) is 40 m^{-3} unless otherwise specified.

In Figs. 5a and 5b the back-scattered flux is plotted as a function of depth for different number densities (N) of fish having $g = 0.5$ and 0.87 respectively. A school fish thickness of 5 m, present at a depth of 10 m from the ocean surface ($L_1 = 10$ m, $L_2 = 5$ m), is considered. The different values of N used are 4, 40, and 400 m^{-3}. The higher the value of N, the higher the scattering coefficient, as can be seen from Eqs. (9a) and (9b). Consequently, the magnitude of the back-scattered signal increases due to the increased scattering events. But at the same time, due to a higher value of attenuation coefficient for the higher value of N, the source pulse decays faster and correspondingly, the back-scattered flux drops off rapidly. In the same figure, the plot of the back-scattered signal from ocean water containing no fish ($N = 0$) is also shown. The measured signal remains the same as that of the no fish case until the signal reaches the school of fish. Since the fish phase function distribution is more backward-directed, and a lower value of g implies broader phase function distribution, the effect of the school's presence is masked in the back-scattered signal distribution, as can be seen in Fig. 5a. Therefore in this section the back-scattered flux distribution is generated for a value of $g = 0.87$.

Figure 6 shows the back-scattered flux distribution for different widths of fish schools ($L_2 = 1$, 5, and 10 m). The smaller the school width, the less is the pulse spreading and magnitude of the flux. The non-dimensional back-scattered flux is plotted in Fig. 7 as a function of depth for different regions where schools of fish are present from the surface of the ocean (L_1). In this case the values of L_1 used are 5, 10, and 15 m. The first significant change in signal is observed corresponding to the depth of the fish from the ocean's surface. The closer the fish from the surface, the faster the decay of the corresponding back-scattered flux.

Another issue worth mentioning is that for highly turbid water, no change in the pattern of the flux distribution is noticeable in the region between the school of fish and absence of fish. This implies that detection of fish in highly turbid water is not possible.

6. CONCLUSIONS

The present study is the first in the literature to simulate detection of a school of fish using transient radiative transfer formulation for signals obtained from oceanographic lidar. The significance of this comprehensive study examining the theoretical and numerical modeling of the transient radiative transport through ocean water is its implications for effective management and control of fisheries. This study highlights the fact that the lidar attenuation coefficient can be less than the diffuse attenuation coefficient contrary to the steady state findings. The advantage of short pulse lidar probing technique is that it provides additional information about the medium properties. The findings will prove to be a valuable tool for efficient analysis of lidar operation. Further research is being conducted for better representation of the particle and fish phase function distribution.

7. ACKNOWLEDGEMENTS

This work was performed while the first author (Kunal Mitra) held a National Research Council-National Oceanic and Atmospheric Administration Research Associateship.

8. REFERENCES

1. C.D. Mobley, B. Gentili, H. Gordon, Z. Jin, G. Kattawar, A. Morel, P. Reinersman, K. Stamnes, R. Stavn, "Comparison of numerical models for computing underwater light fields," *Applied Optics* **32**, pp. 7484-7504, 1993.

2. M.M. Krekova, G.M. Krekov, I.V. Samokhvalov, V.S. Shamanaev, "Numerical evaluation of possibilities of remote laser sensing of fish schools," *Applied Optics* **33**, pp. 5715-5720, 1994.

3. Z. Jin and K. Stamnes, "Radiative transfer in nonuniformly refracting layered media: atmosphere-ocean system," *Applied Optics* **33**, pp. 431-442, 1994.

4. A. Yodh and B. Chance, "Spectroscopy and imaging with diffusing light," *Physics Today* **48**, pp. 34-40, 1995.

5. Y. Yamada, "Light-tissue interaction and optical imaging in biomedicine," *Annual Review of Fluid Mechanics and Heat Transfer (Ed: C.L. Tien)* **6**, pp. 1-59, 1995.

6. S. Kumar, K. Mitra, and Y. Yamada, "Hyperbolic damped-wave models for transient light pulse propagation in scattering media," *Applied Optics* **35**, pp. 3372-3378, 1996.

7. C.D. Mobley, "The optical properties of water," *Handbook of Optics*: Fundamentals, Techniques, Design **1**, Chapter 43, 1995.

8. J.H. Churnside, and J.R. Hunter, "Laser remote sensing of epipelagic fishes," *SPIE* Proceedings-*Laser Remote Sensing of Natural Waters: From Theory to Practice* **2964**, pp. 38-53, 1996.

9. J.H. Churnside, J.J. Wilson, and V.V. Tatarskii, "Lidar profiles of fish schools," *Applied Optics* **36**, pp. 6011-6016, 1997.

10. J.L. Squire, and H. Krumboltz, "Profiling pelagic fish schools using airborne optical lasers and other remote sensing techniques," *Marine Technology Society Journal* **15**, pp. 443-448, 1981.

11. D.L. Murphree, C.D. Taylor, and R.W. McClendon, "Mathematical modeling for the detection of fish by an airborne laser, *AIAA Journal* **12**, pp. 1686-1692, 1974.

12. R. Siegel, and J.R. Howell, *Thermal Radiation Heat Transfer*, McGraw Hill, 1981.

13. G.E. Hunt, "The generation of angular distribution coefficients for radiation scattered by a spherical particle," *Journal of Spectroscopy and Radiative Transfer* **10**, pp. 857-864, 1970.

14. M.F. Modest, *Radiative Heat Transfer*, McGraw Hill, 1993.

15. E. Isaacson, and H.B. Keller, *Analysis of Numerical Methods*, John Wiley, New York, 1966.

16. M.P. Menguc and R. Viskanta, "Comparison of radiative transfer approximations for highly forward scattering planar medium," *Journal of Quantitative Spectroscopy and Radiative Transfer* **29**, pp. 381-394, 1983.

17. S. Kumar, A. Majumdar, and C.L. Tien, "The differential-discrete-ordinate method for solutions of the equation of radiative transfer," *ASME Journal of Heat Transfer*, **112**, pp. 424-429, 1990.

18. N.K. Madsen and R.F. Sincovec, "Algorithm 540 PDECOL, General Collocation Software for Partial Differential Equations [D3]," *ACM Transactions on Mathematical Softwares* **5**, pp. 326-361, 1979.

19. C.D. Mobley, *Light and Water: Radiative Transfer in Natural Waters*, *Academic Press*, 1994.

20. H.R. Gordon, "Sensitivity of radiative transfer to small-angle scattering in the ocean: quantitative assessment," *Applied Optics* **32**, 7505-7511, 1993.

Table 1. Optical properties of different types of water.				
ω	0.245	0.454	0.551	0.833
k_a, m^{-1}	0.114	0.120	0.179	0.366
k_a+k_s, m^{-1}	0.151	0.220	0.398	2.190
g=0.25				
k_d, m^{-1}	0.122	0.179	0.333	1.283
$\hat{k}_d$, m^{-1}	0.126	0.152	0.249	0.947
α, m^{-1}	0.117	0.133	0.201	0.427
g=0.5				
k_d, m^{-1}	0.116	0.167	0.306	1.087
$\hat{k}_d$, m^{-1}	0.120	0.137	0.216	0.677
α, m^{-1}	0.115	0.127	0.197	0.410
g=0.75				
k_d, m^{-1}	0.107	0.150	0.263	0.833
$\hat{k}_d$, m^{-1}	0.117	0.127	0.194	0.487
α, m^{-1}	0.109	0.116	0.185	0.403
g=0.87				
k_d, m^{-1}	0.101	0.133	0.222	0.520
$\hat{k}_d$, m^{-1}	0.115	0.123	0.186	0.442
α, m^{-1}	0.107	0.115	0.182	0.400

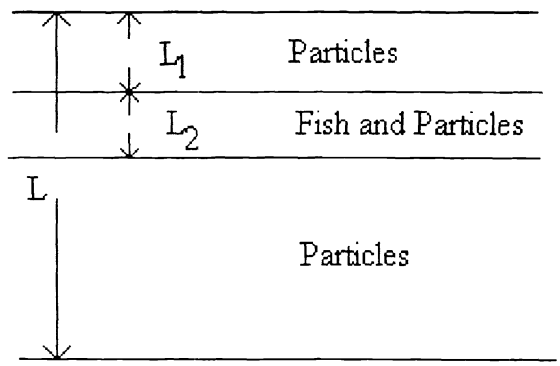

Figure 1. Schematic of the problem under consideration.

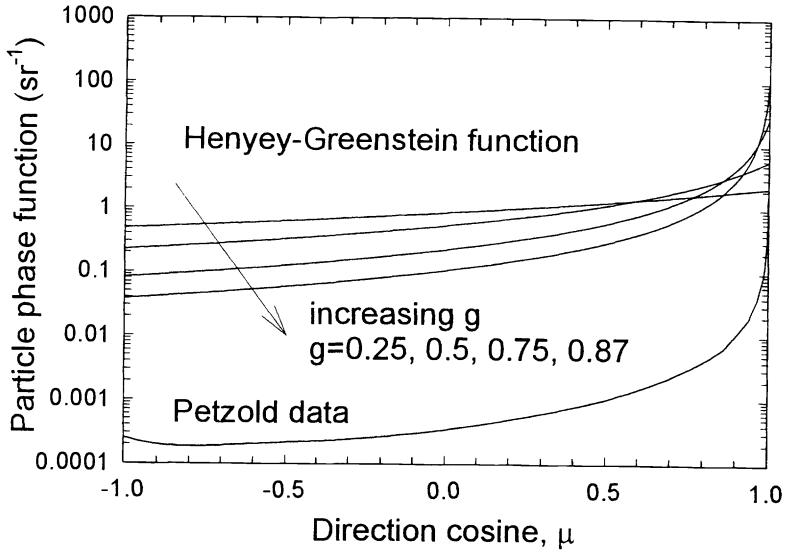

Figure 2. Plot of Petzold phase function and Henyey-Greenstein phase function distribution for different values of asymmetry factor.

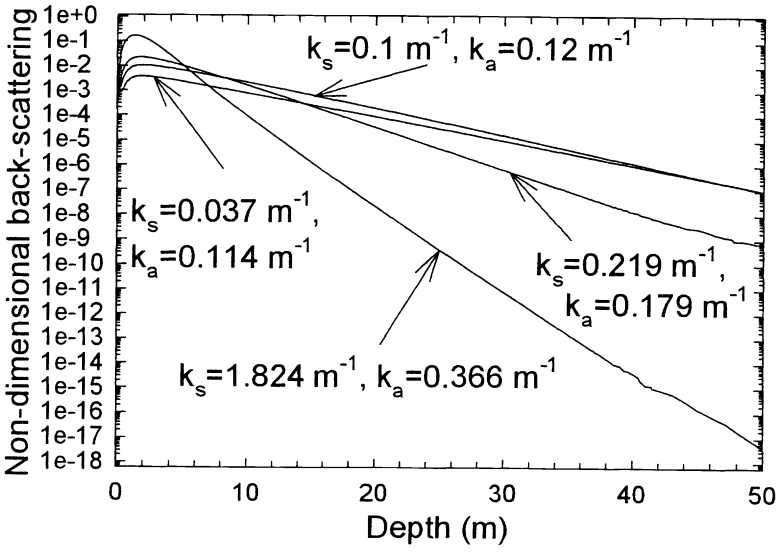

Figure 3. Comparison of the back-scattered signal as a function of depth for various types of ocean water using discrete ordinates method.

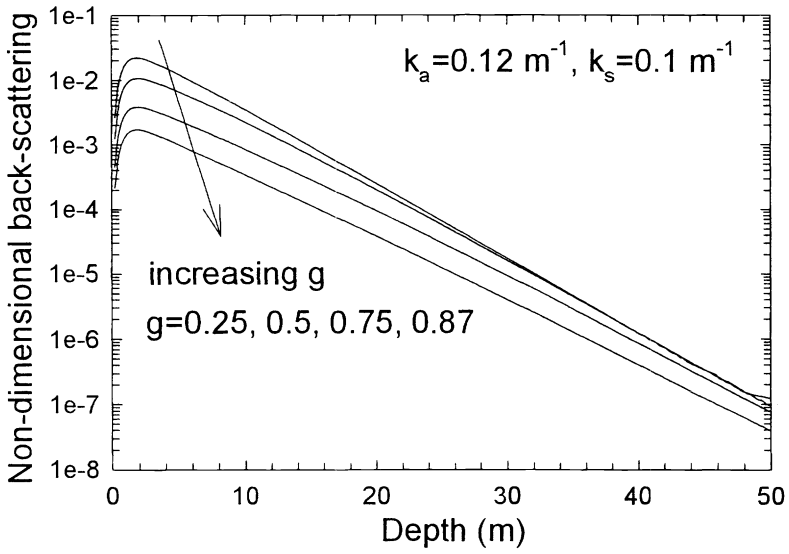

Figure 4. Comparison of the back-scattered signal as a function of depth for various types of phase function using discrete ordinates method.

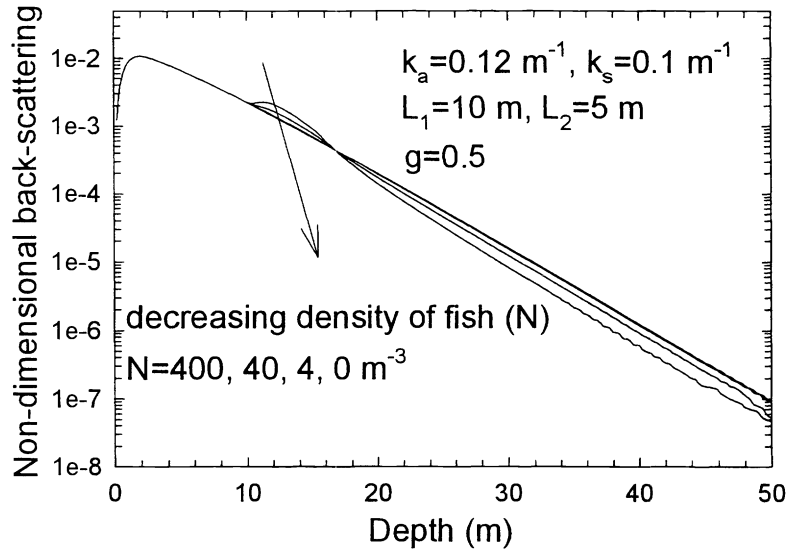

Figure 5a. Comparison of the back-scattered signal as a function of depth for different number density of fish using the discrete ordinates method having g = 0.5.

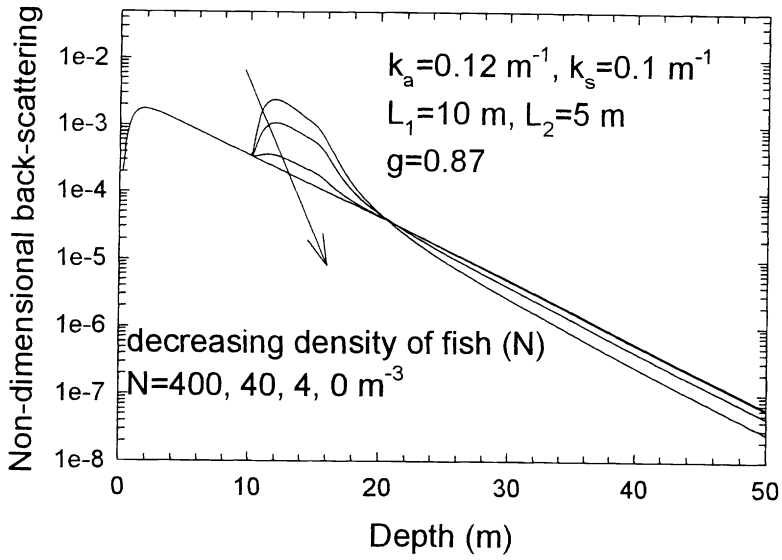

Figure 5b. Comparison of the back-scattered signal as a function of depth for different number density of fish using discrete ordinates method having g = 0.87.

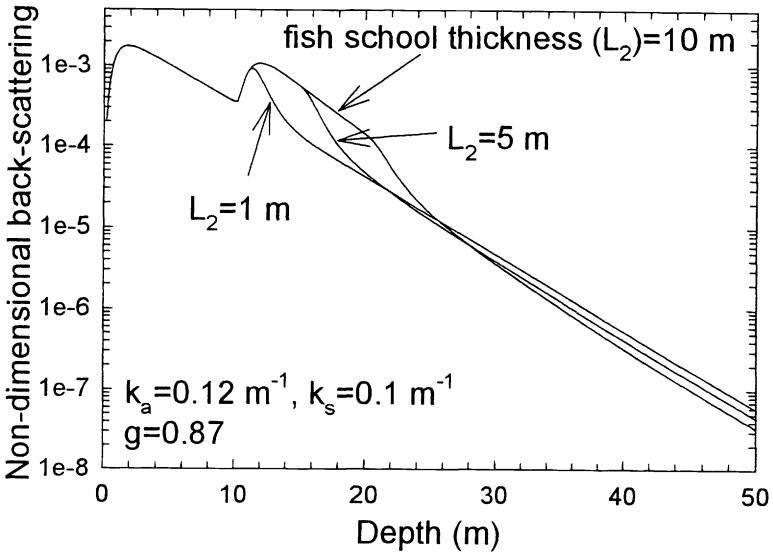

Figure 6. Comparison of the back-scattered signal as a function of depth for different thickness of schools of fish using the discrete ordinates method.

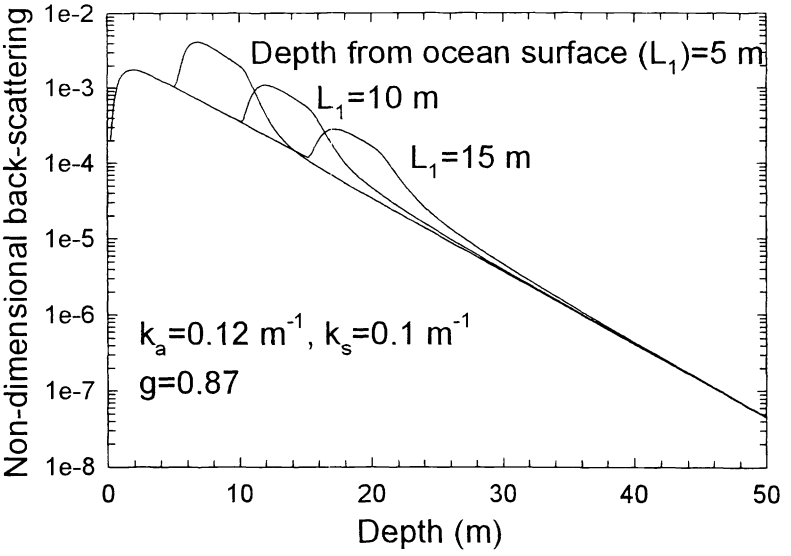

Figure 7. Comparison of the back-scattered signal as a function of depth for different depths from the ocean surface where schools of fish are present using discrete ordinates method.